Structural and Biochemical Studies of Botulinum Neurotoxin Serotype C1 Light Chain Protease: Implications for Dual Substrate Specificity[†,‡]

Rongsheng Jin,[§] Stefan Sikorra,[‖] Christian M. Stegmann,[§] Andreas Pich,[⊥] Thomas Binz,[‖] and Axel T. Brunger*,[§]

Howard Hughes Medical Institute and Departments of Molecular and Cellular Physiology, Neurology and Neurological Sciences, Structural Biology, and Stanford Synchrotron Radiation Laboratory, Stanford University, Stanford, California 94305, and Institutes of Biochemistry and Toxicology, Medical School Hannover, 30623 Hannover, Germany

ABSTRACT: Clostridial neurotoxins are the causative agents of the neuroparalytic disease botulism and tetanus. They block neurotransmitter release through specific proteolysis of one of the three soluble *N*-ethylmaleimide-sensitive-factor attachment protein receptors (SNAREs) SNAP-25, syntaxin, and synaptobrevin, which constitute part of the synaptic vesicle fusion machinery. The catalytic component of the clostridial neurotoxins is their light chain (LC), a Zn^{2+} endopeptidase. There are seven structurally and functionally related botulinum neurotoxins (BoNTs), termed serotype A to G, and tetanus neurotoxin (TeNT). Each of them exhibits unique specificity for their target SNAREs and peptide bond(s) they cleave. The mechanisms of action for substrate recognition and target cleavage are largely unknown. Here, we report structural and biochemical studies of BoNT/C1-LC, which is unique among BoNTs in that it exhibits dual specificity toward both syntaxin and SNAP-25. A distinct pocket (S1′) near the active site likely achieves the correct register for the cleavage site by only allowing Ala as the P1′ residue for both SNAP-25 and syntaxin. Mutations of this SNAP-25 residue dramatically reduce enzymatic activity. The remote α-exosite that was previously identified in the complex of BoNT/A-LC and SNAP-25 is structurally conserved in BoNT/C1. However, mutagenesis experiments show that the α-exosite of BoNT/C1 plays a less stringent role in substrate discrimination in comparison to that of BoNT/A, which could account for its dual substrate specificity.

The clostridial neurotoxins (CNTs[1]) are synthesized by the Gram-positive soil bacteria *Clostridium botulinum* and *Clostridium tetani* and are among the most lethal neurotoxins (*1*). The estimated 50% lethal dose (LD_{50}) of botulinum neurotoxin serotype C1 (BoNT/C1) in mice is approximately 1 ng per kg of body weight when administered intravenously (*2*). CNTs could thus potentially be used as a biological weapon, since they can be easily produced, transported, and efficiently delivered via aerosol or liquid routes (*3*, *4*). In spite of their extreme toxicity, a growing number of applications are emerging for clinical treatment of certain neurological disorders by CNTs (*5*).

The CNTs are synthesized as single polypeptide chains of approximately 150 kDa. This single chain is post-translationally cleaved by some bacterial and tissue proteases into a 50 kDa light chain (LC) that contains a Zn^{2+}-dependent endopeptidase, and a 100 kDa heavy chain (HC) that is responsible for highly specific host cell binding and internalization. Upon cleavage, the LC and HC of CNTs remain covalently and reversibly linked by a disulfide bond until being exposed to reducing conditions, such as the nerve cytosol (see ref *6* for review). The CNT-LCs cleave specific peptide bonds within the neuronal SNARE proteins (synaptobrevin, syntaxin, and SNAP-25). BoNT/A and E specifically cleave SNAP-25 while serotypes B, D, F, and G of BoNTs cleave synaptobrevin. BoNT/C1 is unique in that it is able to hydrolyze two substrates: syntaxin (*7*, *8*) and SNAP-25 (*9−11*). Syntaxin is cleaved by BoNT/C1 between residues Lys253 and Ala254 (*8*), whereas SNAP-25 cleavage occurs between Arg198 and Ala199 (*11*).[2]

The CNT-LCs are highly specific proteases. For example, the scissile bond in SNAP-25 for BoNT/A (Gln197−Arg198) is shifted by only one residue compared to that for BoNT/C1 (Arg198−Ala199). Only one of two identical neighboring peptide bonds (Lys253−Ala254 and Lys260−Ala261) in syntaxin-1A is cleaved by BoNT/C1 (*8*). Furthermore, unusually long stretches of residues of the substrates are required for optimal cleavage, and point mutations in

---

* Correspondence: brunger@stanford.edu. Tel: (650) 736-1031. Fax: (650) 736-1961.

[§] Howard Hughes Medical Institute and Departments of Molecular and Cellular Physiology, Neurology and Neurological Sciences, Structural Biology, and Stanford Synchrotron Radiation Laboratory, Stanford University.

[‖] Institute of Biochemistry, Medical School Hannover.

[⊥] Institute of Toxicology, Medical School Hannover.

[1] Abbreviations: SNAREs, soluble *N*-ethylmaleimide-sensitive-factor attachment protein receptor; BoNTs, botulinum neurotoxins; TeNT, tetanus neurotoxin; LC, light chain; HC, heavy chain; CNTs, clostridial neurotoxins.

---

[2] BoNT/C1 should not be confused with *Clostridium botulinum* C2 toxin, which is a two-component toxin that exerts its toxicity by ADP-ribosylation of G-actin 12 (Aktories, K., and Barth, H. (2004) The actin-ADP-ribosylating Clostridium botulinum C2 toxin, *Anaerobe 10*, 101−105) and thus is not considered a CNT.

SNAREs far remote from the scissile bond can dramatically reduce the proteolysis efficiency (*11*, *13*, *14*). The structure of the BoNT/A-LC·SNAP-25 complex has provided the first structural insights at the extraordinary substrate specificity of BoNTs by identifying an array of substrate recognition sites located remote from the active site, termed exosites (*14*). However, it is unknown if other CNTs exploit a similar mechanism for substrate recognition.

SNAREs exhibit considerable conformational variability; they can exist as monomeric components with little secondary structure, as (partially) structured SNARE complexes or subcomplexes, or as part of complexes with regulatory factors (*15*). BoNT/C1 interacts with specific pools of SNAP-25 and syntaxin, as suggested by the following observations: BoNT/C1 cleaves SNAP-25 at higher efficiency in living neurons in comparison to *in vitro* cleavage (*10*), and BoNT/C1 cleaves syntaxin only when syntaxin is inserted into a lipid bilayer *in vitro* (*8*). Clinically, BoNT/C1 is a potential therapeutic alternative to BoNT/A treatment for patients who are nonresponders to BoNT/A (*16*, *17*). A recent clinical study applying BoNT/C1 to BoNT/A-resistant patients suffering from blepharospasm and cervical dystonia reported a good clinical response and no collateral or adverse effects (*18*), despite the fact that BoNT/C1 can impair neurite/axonal growth and cause neuronal cell death which is associated with the cleavage of syntaxin (*19*). Thus, a better understanding of the mechanism of substrate recognition and cleavage for BoNT/C1 is highly desirable. Here we present the crystal structure of BoNT/C1-LC at 1.75 Å resolution, along with mutagenesis experiments of the SNAP-25 substrate. Comparison with BoNT/A reveals both conserved and divergent features that provide a basis for understanding the scissile bond recognition and the dual substrate specificity of BoNT/C1.

MATERIALS AND METHODS

Protein Purification. A BoNT/C1-LC construct comprising residues 1−430 with a thrombin-cleavable C-terminal hexahistidine affinity tag was generated and cloned into a pQE vector (Qiagen). Recombinant BoNT/C1-LC was expressed in *Escherichia coli* strain M15[pREP4] cells (Qiagen). Bacteria were grown at 37 °C and induced with 250 μM isopropyl-β-D-thiogalactopyranoside (IPTG) when OD_{600} absorption reached 0.8−1.0 in TB medium. The temperature was then reduced to 20 °C, and the induction was continued for ∼16 h. Cells were lysed via two passes through a M-110EH Microfluidizer Processor (Microfluidics) at 18,000 psi. Phenylmethylsulfonyl fluoride (PMSF, 1 mM) was added to the lysate as a protease inhibitor. Insoluble debris was removed from the lysate by centrifugation in a Ti-45 rotor (Beckman) at 40,000 rpm for 45 min. Affinity purification was performed using Ni−nitrilotriacetic acid−agarose (Ni-NTA) resin (Qiagen) according to the manufacturer's instructions. The His-tag was removed with bovine α-thrombin (Haematologic Technologies), and additional purification was achieved with cation-exchange chromatography (Mono-S column, GE Healthcare) at pH 7.4. BoNT/C1-LC was quantified by UV/vis spectroscopy at 280 nm, based on its theoretical extinction coefficient in denaturing conditions (42100 M^{-1} cm^{-1}). The expected molecular mass of the protein was confirmed using a MALDI mass spectrometer (Bruker).

SNAP-25 and its mutants with C-terminal hexahistidine affinity tag (SNAP-25His$_6$) were expressed utilizing the *E. coli* strain M15pREP4 (Qiagen) with 5 h of incubation at 30 °C and purified on Ni-NTA beads (Qiagen). Proteins were dialyzed against toxin assay buffer (150 mM K-glutamate, 10 mM HEPES-KOH, pH 7.2), frozen in liquid nitrogen, and kept at −70 °C. BoNT/C1-LC (1−449) and BoNT/A-LC (1−449) were produced as previously described (*11*) .

Crystallization and Diffraction Data Collection. The purified BoNT/C1-LC was dialyzed against a buffer containing 20 mM Hepes (pH 7.4) and then concentrated to about 12 mg/mL for crystallization. Initial crystallization screens were carried out using the Phoenix crystallization robot (Art Robbins Instruments) and high throughput crystallization screen kits from Hampton Research, Emerald Biostructures, and Qiagen. The best crystals were grown at 4 °C by vapor diffusion with a 1:1 (v/v) ratio of protein and reservoir solution containing 1.6 M sodium formate and 0.1 M sodium citrate (pH 4.6−5.0). The crystals were cryoprotected in the same mother liquor supplemented with 20% glycerol, and then flash-frozen in liquid nitrogen. Diffraction data were collected at 100 K at beam line 9-2, Stanford Synchrotron Radiation Laboratory (SSRL), using a Mar-325 CCD detector. All data were processed using HKL2000 (Table 1) (*20*). The crystals belong to space group $P3_121$, with unit cell dimensions $a = b = 107.0$ Å, $c = 140.4$ Å, $\gamma = 120°$ and diffracted to 1.75 Å resolution.

Structure Determination. The structure of BoNT/C1-LC was determined by molecular replacement using Phaser (*21*). The structures of BoNT/A-LC (PDB code 1XTF) (*14*) and BoNT/D-LC (PDB code 2FPQ) (*22*) both yielded unambiguous and significant solutions when used as search models (the sequence identities for the LCs of BoNT/C1 vs A and BoNT/C1 vs D are 32% and 47%, respectively). The MR solution using the BoNT/D-LC search model was chosen for further model building and structure refinement. Manual model building was performed with Coot (*23*), and all the refinements were carried out with the Crystallography & NMR System (CNS), version 1.2 (*24*). Progress was monitored with the free *R*-value using a 10% randomly selected test set (*25*). Refinements were begun with rigid body minimization followed by a slow-cooling simulated annealing protocol at 5000 K to reduce model bias. Iterative rounds of positional and individual *B*-factor refinement were performed in conjunction with manual model building until R_{free} converged. Superimposition of structures was carried out using LSQMAN (*26*) or SSM Superposition (*27*). Figures were prepared with PyMol (http://www.pymol.org) and Povscript+ (*28*).

Endopeptidase Assay. In standard time course assays, SNAP-25His$_6$ or its mutants (10 μM for BoNT/C1-LC; 5 μM for BoNT/A-LC) were incubated in the presence of 550 nM and 1 nM final concentrations of BoNT/C1-LC or BoNT/A-LC, respectively, in a total volume of 100 μL of toxin assay buffer (see Protein Purification) at 37 °C. 15 μL aliquots were withdrawn at specified time intervals. Reactions were stopped by mixing with 15 μL of ice-cold double concentrated sample buffer (120 mM Tris-HCl pH 6.75, 10% (v/v) β-mercaptoethanol, 4% (w/v) SDS, 20% (w/v) glycerol, 0.014% (w/v) bromphenol blue). Samples were subjected to SDS−PAGE on 12.5% gels. Proteins were visualized by staining with Coomassie Blue and quantified with a LAS-

Table 1: Crystallographic Data

Data Collection			
wavelength (Å)	1.192	solvent content (%)	71.0
space group	$P3_121$	resolution (Å)[b]	40.0 − 1.75
unit cell parameters		total reflections	640,609
a (Å)	107.0	unique reflections	86,796
b (Å)	107.0	multiplicity	7.4
c (Å)	140.4	completeness (%)[b]	92.4 (55.6)
γ (deg)	120	R_{sym} (%)[b,c]	7.5 (39.9)
molecules per AU[a]	1	average $I/\sigma(I)$[b]	26.5 (2.5)
Refinement			
resolution range (Å)	40.0−1.75	protein residues	429
R_{free}/R_{work}[d]	20.5/18.8	Zn^{2+} ions	1
rmsd, bonds (Å)	0.005	water molecules	626
rmsd, angles (deg)	1.27	average B factors (Å²)	27.4
Ramachandran Analysis[e]			
most favored	337	generously allowed	0
additionally allowed	46	disallowed	1

[a] AU: asymmetric unit. [b] Numbers in parentheses represent the highest resolution bin. [c] $R_{sym} = \sum_h\sum_i|I_{hi} - \langle I_h\rangle|/\sum_h\sum_i|I_{hi}|$. [d] $R_{work} = (\sum||F_o| - |F_c||)/\sum|F_o|$, where F_o and F_c denote observed and calculated structure factors, respectively. Ten percent of the reflections were set aside for calculation of R_{free}. [e] Number of non-proline and non-glycine residues.

3000 image reader employing the AIDA program (version 2.11; raytest Isotopenmessgeräte, Straubenhardt, Germany).

For the determination of the enzyme kinetic parameters of selected SNAP-25 mutants, the substrate concentration was varied between 1.0 and 60 μM. Each of the various substrate concentrations was endowed by the addition of 1 μL of radiolabeled SNAP-25His$_6$ or its mutants generated by *in vitro* transcription/translation. Incubation was done in a final volume of 30 μL of toxin assay buffer. After 10 and 15 min of incubation at 37 °C, aliquots of 10 μL were taken and the enzymatic reaction was stopped by mixing with 10 μL of prechilled double concentrated SDS−PAGE sample buffer. SNAP-25 and its cleavage product were separated by SDS−PAGE, and radiolabeled protein was visualized using a BAS-1500 phosphor imager (Fuji Photo Film, Japan). The percentage of hydrolyzed SNAP-25 was determined from the turnover of the radiolabeled substrate applying the Tina 2.09f program (Raytest Isotopenmessgeräte) and used to calculate the initial velocity of substrate hydrolysis. K_m and V_{max} values were derived from Lineweaver−Burk plots using the GraphPad Prism 4.03 program (GraphPad Software Inc, San Diego, U.S.A.).

Mass Spectrometry. N-terminal cleavage products obtained from Coomassie Blue-stained polyacrylamide gels were identified after tryptic digestion in a MALDI-TOF mass spectrometer (Ultraflex I, Bruker Daltonics, Bremen, Germany). Briefly, bands were cut out of the gel, destained using 50% acetonitrile, and dried by addition of 100% acetonitrile and incubation in a speed vac system. Trypsin solution (10 ng/μL) was added to the dried gel piece. After overnight incubation at 37 °C, peptides were extracted from the gel using 5% TFA containing 10% acetonitrile. Extraction solutions were dried and dissolved in 0.2% TFA, 50% acetonitrile. Samples were mixed with 1 μg of α-cyano-4-hydroxycinnamonic acid (CHCA), dissolved in 0.2% TFA and 50% acetonitrile and applied to the MALDI target. MS and MS/MS spectra were collected and all data were analyzed using the Biotools (Bruker Daltonic) and MASCOT (Matrix Science, U.K.) software packages.

To identify the C-terminal cleavage products wild-type and mutated SNAP-25 were incubated with BoNT/C1-LC. After termination of the reaction, peptides were isolated and

desalted using ziptips containing a c18 phase (Millipore Corporation, USA). Ziptips were activated with 30 μL of acetonitrile and equilibrated with 30 μL of 5% acetonitrile, 0.2% TFA. Subsequently, the reaction mixture was applied to the ziptips. After washing with 30 μL of 5% acetonitrile, 0.2% TFA, peptides were eluted with 5 μL of 60% acetonitrile, 0.2% TFA, applied to the MALDI target and analyzed as outlined above.

RESULTS AND DISCUSSION

Structure of BoNT/C1-LC. A slightly truncated construct of BoNT/C1-LC (1−430) was designed based on homology modeling with the crystal structure of BoNT/A-LC and secondary structure prediction (simply referred to as BoNT/C1-LC). This construct has a similar SNAP-25 cleavage activity when compared with full-length BoNT/C1-LC (1−449) (data not shown). The crystal structure of this BoNT/C1-LC construct was determined to 1.75 Å resolution with one monomer per asymmetric unit (Figure 1A and Table 1). Electron density was clearly visible for all residues except for the very N-terminus. The catalytic zinc ion was readily found in an anomalous difference Fourier map (Figure 3A). Despite their different substrate specificities, the overall structure of BoNT/C1-LC is similar to those of other CNT-LCs as reflected by high DALI Z-scores (29) (Figure 1B). The Z-scores are 45.8, 47.8, 52.5, 46.4, 47.8, 47.0, and 47.9 for serotypes A, B, D, E, F, G, and TeNT, respectively (it should be noted that pairs with Z-scores of 2.0 are already considered to be structurally similar). The structural differences among the CNT-LCs are mostly limited to solvent-exposed loops. When compared with the structure of BoNT/A-LC, the loops with the largest differences comprise residues 24−32, 47−58, 118−132, 137−146, 203−219, 250−263, and 310−318 (colored blue in Figure 1A).

The "closed" conformation of residues 248−266 (termed the 250-loop) of BoNT/C1-LC is unique among all apo structures of CNTs, in that it is similar to the conformation of the corresponding loop adopted by BoNT/A-LC upon substrate binding (14). This closed conformation of the 250-loop anchors the SNAP-25 substrate at its C-terminal side to BoNT/A-LC by forming a small antiparallel β-sheet
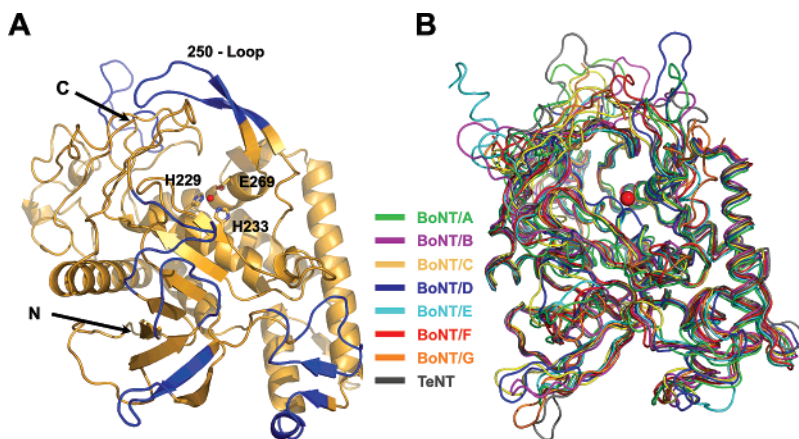
FIGURE 1: Crystal structure of BoNT/C1-LC. (A) Ribbon diagram of BoNT/C1-LC. Also shown are the active site residues (His229, His233, and Glu269) (balls-and-sticks) that coordinate the zinc ion (red sphere). Regions that show large conformational differences in comparison to the structure of BoNT/A-LC, including residues 24−32, 47−58, 118−132, 137−146, 203−219, 250−263, and 310−318, are colored in blue. (B) An overall Cα atom alignment of the light chain structures from all seven serotypes of BoNTs and TeNT: BoNT/A (PDB code 1XTF, green) (*14, 36, 37*), BoNT/B (1F82, magenta) (*38*), BoNT/C1 (gold), BoNT/D (2FPQ, blue) (*22*), BoNT/E (1T3A, cyan) (*39*), BoNT/F (2A8A, red) (*33*), BoNT/G (1ZB7, orange) (*34*), and TeNT (1Z7H, gray) (*40*). Despite their different substrate specificities, CNT-LCs display high structural similarity.
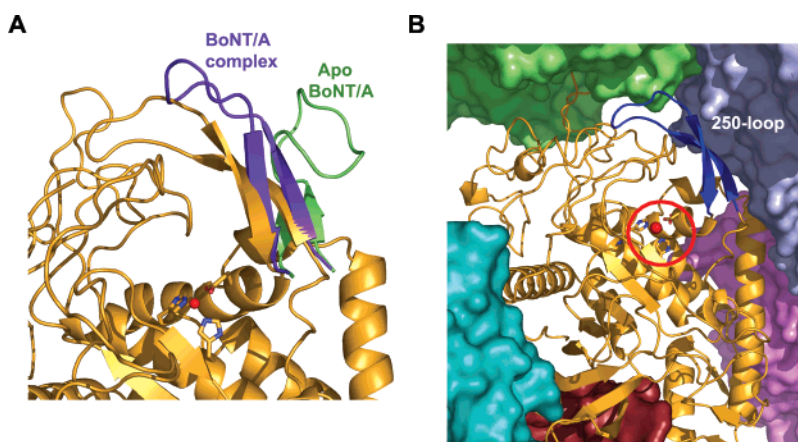

FIGURE 2: The closed conformation of the 250-loop of BoNT/C1-LC. (A) Superimposed structures of BoNT/C1-LC (gold), BoNT/A-LC apo (1XTF, green), and BoNT/A-LC·SNAP-25 complex (1XTG, purple). Close-up view around the 250-loops is shown in an orientation similar to that of Figure 1A. (B) Crystal packing. Ribbon diagram of BoNT/C1-LC is colored in gold while the 250-loop is in blue. Molecular surfaces of all adjacent symmetry mates of the BoNT/C1-LC structure are shown in different colors. The 250-loop of BoNT/C1-LC is involved in crystal contacts, while its active site (highlighted with a red circle) is fully exposed to solvent.

(Figure 2A). In contrast, in the other known structures of CNT-LCs, this loop is in an "open", more unstructured state similar to that of apo BoNT/A, and often associated with weak electron density. It should be noted, however, that the closed conformation of the 250-loop of apo BoNT/C1-LC might have been influenced by crystal packing and is not identical to the substrate-bound conformation of BoNT/A-LC (Figure 2B).

Active Site of BoNT/C1-LC. The active site of BoNT/C1-LC has the same geometry and coordination of the catalytic zinc-binding HExxH motif as that found in the structures of all other CNT-LCs. A zinc ion is coordinated by residues His229, His233, Glu269 and by a water molecule that may act as a nucleophile during catalysis (Figure 3A). A second zinc ion has been observed by atomic adsorption in natively purified full-length BoNT/C1 (*8*). However, careful evaluation of an anomalous difference Fourier map did not provide any evidence for a second zinc ion in the BoNT/C1-LC structure. Considering the hypothesized structural function of this second zinc ion, it is unlikely to dissociate during

protein purification. We thus conclude that this second zinc ion binds to a region other than the LC.

Unlike previously reported CNT-LC apo structures, the active site in BoNT/C1-LC is fully solvent exposed in the context of the crystal lattice (Figure 2B), therefore rendering this crystal form of BoNT/C1-LC a potential target for soaking experiments with small molecule inhibitors. Interestingly, the cocrystal structures of L-arginine hydroxamate both with wild type and with a double-mutant of BoNT/A-LC also have an unobstructed active site (*30, 31*).

S1′ Pocket of BoNT/C1-LC. CNTs have a strict dependence on the P1′ residues of their substrates (*11*). Our structural and biochemical data now shed light on the recognition of the P1′ residue by BoNT/C1-LC. We first compared the structures of BoNT/C1-LC and the thermolysin·ZFPLA-inhibitor complex (PDB code 4TMN) (*32*). CNT-LCs share a similar catalytic core structure with the zinc metalloprotease thermolysin and ZFPLA is a transition state analogue for thermolysin which contains a leucine residue at the P1′ site (*22, 33−35*). By superimposing the HExxH
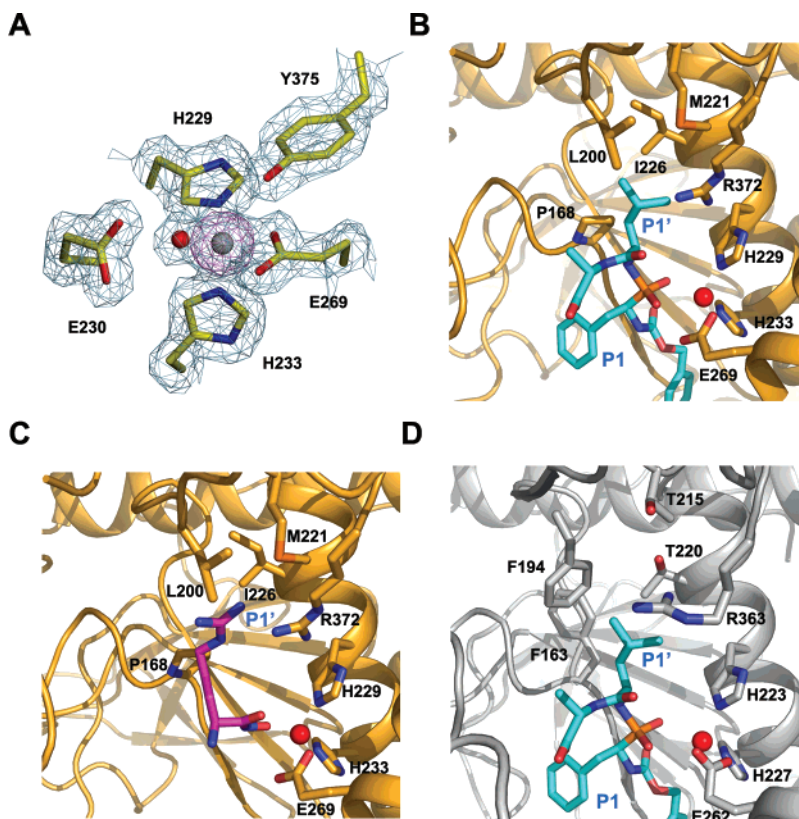
FIGURE 3: The active site and the putative S1′ subsite of BoNT/C1-LC. (A) The active site residues near the catalytic zinc are shown along with a cross-validated, $2F_o - F_c$ σ_A-weighted electron density map contoured at 1σ (gray mesh) and an anomalous difference map (violet mesh). A strong anomalous peak confirms the position of the catalytic zinc ion (gray sphere). A water molecule (red sphere) also coordinates the zinc ion. (B) The putative S1′ pocket of BoNT/C1-LC with a modeled transition state analogue (ZFPLA) of thermolysin containing Leu and Phe at the P1′ and P1 sites, respectively (PDB code 4TMN). BoNT/C1-LC is colored gold, the ZFPLA molecule is colored cyan, and the active site zinc ion is colored red. (C) The putative S1′ pocket of BoNT/C1-LC with a modeled BoNT/A inhibitor ArgHX with an Arg at the P1′ site (PDB code 2G7Q) (*30*). BoNT/C1-LC is colored similarly as that in panel (B), and ArgHX is colored red/purple. The putative S1′ subsite of BoNT/A-LC based on structural comparison with thermolysin·ZFPLA complex is shown in panel (D) while BoNT/A-LC is in gray.

motifs of these two structures, we identified a putative S1′ pocket in BoNT/C1-LC, composed of residues Pro168, Leu200, Met221, Ile226, His229, and Arg372 (Figure 3B). We came to the same conclusion when superimposing the structure of BoNT/C1-LC and that of an inactive double-mutant BoNT/A-LC (Arg362Ala and Tyr365Phe) in complex with the inhibitor L-arginine hydroxamate (ArgHX) (Figure 3C) (*30*) as well as that of ArgHX with wild-type BoNT/A-LC (*31*). This putative S1′ pocket in BoNT/C1-LC is smaller than that in BoNT/A-LC, partially due to the intrusion of the Met221 side chain into this cavity, as compared to the corresponding residue in BoNT/A (Thr215) (Figure 3D). The distances between the CG atom of Thr215[BoNT/A−LC] and the CD atom of Leu[ZFPLA] and between the CG atom of Thr215[BoNT/A−LC] and the NH atom of Arg[ArgHX] are 6.6 Å and 5.3 Å, respectively. In contrast, the corresponding distances involving Met221 of BoNT/C1-LC are only 4.7 Å and 3.2 Å respectively, using the SD atom of Met221 as a reference. In support of our model, both SNAP-25 and syntaxin have a conserved Ala residue at the P1′ site for BoNT/C1 cleavage. Clearly, the small S1′ pocket of BoNT/C1-LC would have a preference for a small side chain at the P1′ position. Thus, the interactions between the P1′ residue and the S1′ pocket could determine the correct register for cleavage by BoNT/C1-LC. In contrast, Arg198 as the P1′ residue of SNAP-25 for BoNT/A cleavage could readily fit into a larger S1′ cavity of BoNT/A-LC (*34*).

To confirm this hypothesis, we substituted Ala199 of SNAP-25 with Gly, Ser, Val, and Arg. The Ala199Gly, Ala199Ser, and Ala199Val mutations all significantly diminished the cleavability of SNAP-25 (Table 2). Most significantly, SNAP-25-Ala199Arg was not cleavable by BoNT/C1 at all. We observed a 3-fold decrease in K_{cat} with SNAP-25-Ala199Ser in comparison to wild-type SNAP-25, with no significant change in K_M. MALDI-MS and MS− MS analyses confirmed that none of these mutations shifted the position of the scissile bond in SNAP-25 (data not shown). Therefore, the P1′ side chain probably aligns the scissile bond with the catalytic motif of the enzyme via its interactions with the corresponding S1′ pocket and therefore directly contributes to the catalytic process. The different composition of the S1′ pockets for BoNT/A and C1 could thus account for the register shift of the cleavage bond of SNAP-25. The S1′ pockets of CNTs are thus part of a network of specific interactions close to the active site.

The residues at the P1 position of the substrate are generally less critical for the enzymatic activity of CNT-LCs than those at the P1′ position (*11*). However, BoNT/C1 is unique among the CNTs in that specific residues, a positively charged Arg or Lys, must be present in the P1 position of SNAP-25 or syntaxin for full activity (*11*). Interestingly, syntaxin-4 that has an Ile at the P1 site is insusceptible to BoNT/C1 (*8, 11*).

Table 2: Endopeptidase Assay

	BoNT/C1-LC							BoNT/A-LC cleavability[a]
mutation	K_M (μM)	SD	K_{cat} (1/min)	SD	K_{cat}/K_M	no. of expts	cleavability[a]	
WT	18.6	5.5	0.391	0.093	0.021	8	100	100
A199G							46.9	
A199S	14.5	5.6	0.136	0.036	0.009	5	23.5	
A199R							not cleavable	
A199V							57.5	
Q152A	34.9	6.7	0.534	0.020	0.015	3	71.1	97.4
Q152R							66.4	112.6
V153A							99.3	90.5
I156A							111.8	54.8
I156E							142.4	45.6
L160E							134.1	6.1
D166A	27.0	1.2	0.512	0.149	0.019	3	69.4	107.4
D166R							82.6	54.5
M167A							116.8	89.9
M167R							122.1	2.8
Δ149−167[b]							71.7	not detectable[d]
186-G-187[c]							115.5	94.5
186-SG-187[c]							125.7	99.5
186-SGS-187[c]	16.6	6.3	0.367	0.082	0.022	5	92.7	97.2
Δ187[b]	14.8	1.4	1.348	0.230	0.091	7	205.6	92.9
Δ187−188[b]	13.0	3.9	0.755	0.269	0.058	6	184.5	92.2
Δ187−189[b]	11.5	3.5	0.319	0.085	0.028	4	127.2	99.8

[a] Percentage of cleavage at 30 min of reaction compared with wild-type SNAP-25. The complete time course data are presented in supplementary Figure 1. [b] Deletion mutants. [c] Insertion between residue Asp186 and Ser187. [d] At standard conditions. 100 nM BoNT/A-LC yielded approximately 84% cleavage within 1 h of incubation.

Putative α-Exosite of BoNT/C1. The structure of the complex between BoNT/A-LC and SNAP-25 revealed an array of remote exosites, which serve to specifically position the substrate in an optimal orientation relative to the active site of BoNT/A-LC (*14*). Similar to BoNT/A-LC, a long stretch of SNAP-25 including residues (93−202) is required to achieve optimum enzymatic activity for BoNT/C1-LC (*11, 35*), suggesting the presence of remote exosites in BoNT/C1 as well. In order to study the structural basis of the substrate specificity of BoNT/C1-LC, we superimposed the BoNT/C1-LC structure with the structure of BoNT/A-LC·SNAP-25 complex (PDB code 1XTG) based on Cα atoms of the two LCs. Remarkably, many of the BoNT/A-LC residues of the α-exosite that are in contact with SNAP-25 are conserved in BoNT/C1-LC (Figure 4). The conformation of SNAP-25 residues as found in the structure of the BoNT/A-LC·SNAP-25 complex can be docked to the putative α-exosite of BoNT/C1-LC, with relatively minor clashes involving BoNT/C1-LC residues Glu353 and Arg331 that can be relieved by side chain rotamer changes (data not shown). Furthermore, the α-exosite-interacting residues are fairly conserved among syntaxin and SNAP-25 (Figure 5A).

Based on the structural comparison between BoNT/C1-LC and the BoNT/A-LC·SNAP-25 complex, we mutated selected residues of SNAP-25 in order to determine if BoNT/C1-LC and BoNT/A-LC share similar interactions at the α-exosite. As expected from previous work (*14*), mutation of Ile156, Leu160, and Met167 significantly reduced cleavability by BoNT/A-LC, whereas mutation of Gln152, Val153, and Asp166 had little effect (Table 2). In contrast, mutation of Val153, Ile156, Leu160, and Met167 did not decrease SNAP-25 cleavability by BoNT/C1-LC, but mutation of Gln152 and Asp166, which potentially form hydrogen bonds with Lys365 and Lys346 of BoNT/C1 (equivalent to Lys356
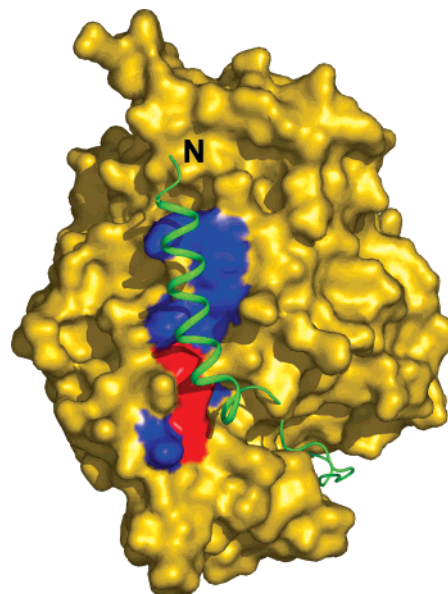

FIGURE 4: Key residues of BoNT/A-LC that interact with the α-exosite of SNAP-25 are mostly conserved in BoNT/C1-LC. A molecular surface of BoNT/C1-LC is colored according to sequence conservation between BoNT/A-LC and BoNT/C1-LC (conserved and nonconserved residues in BoNT/C1-LC are highlighted in blue and red, respectively). The SNAP-25 substrate (green) was modeled based on the crystal structure of the BoNT/A-LC·SNAP-25 complex. The orientation of this figure is rotated by 180° around a vertical axis from that shown in Figure 1A.

and Lys337 of BoNT/A), decreased cleavability by approximately 30%. Kinetic studies with the SNAP-25-Gln152Ala or SNAP-25-Asp166Ala mutants showed primarily increased K_M values, arguing for a role of these residues in productive substrate binding (Table 2). In line with these findings, SNAP-25 lacking the entire α-exosite (residues
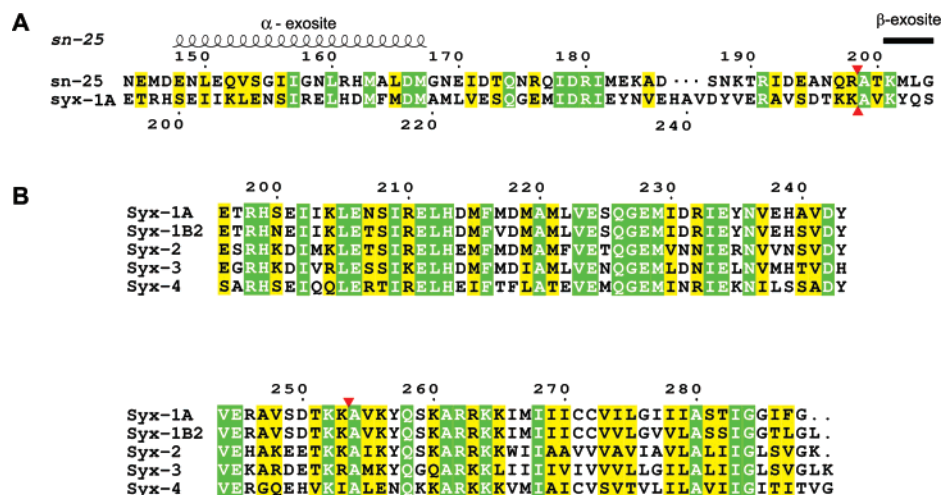
FIGURE 5: Sequence alignments between rat SNAP-25 (sn-25) and syntaxin (syx) (A), and among the four isoforms of rat syntaxin (B). Alignments were performed separately for regions around the α-exosite binding region and around the scissile bond/β-exosite. Identical and similar residues are shown in green and yellow, respectively. The α- and β-exosite binding regions of SNAP-25 in complex with BoNT/A-LC are shown on the top. The BoNT/C1 scissile bonds on SNAP-25 and syntaxin are indicated by red triangles. The sequence alignments were generated by ClustalW (*41*) and ESPript (*42*).

149−167) was cleaved approximately 100-fold less efficiently by BoNT/A-LC whereas the reduction of cleavability by BoNT/C1-LC showed a similar level as that observed for the mutations of Gln152 and Asp166 (Table 2). Thus, the putative α-exosite of BoNT/C1 likely recognizes SNAP-25 and syntaxin in a manner similar to what was observed between BoNT/A and SNAP-25. However, there are differences in detail, and the α-exosite interactions for BoNT/C1 are less stringent than that for BoNT/A. This observation is consistent with the dual substrate specificity of BoNT/C1 considering the sequence differences between SNAP-25 and syntaxin in the α-exosite binding region (Figure 5). The strict requirement for the position of the cleavage bond is thus likely conferred by interactions involving the S1′ pocket and scissile bond proximal exosites. Since the optimal subset of SNAP-25 for BoNT/C1 (93−202) is longer than that for BoNT/A (146−202) (*11*), BoNT/C1 might also exploit additional remote exosites on SNAP-25 that have not been observed in the BoNT/A-LC·SNAP-25 complex.

The Correlation between the α-Exosite and the Scissile Bond Proximal Exosites. In contrast to the conserved structure of the putative α-exosite, the β-exosite and other substrate anchor points for BoNT/A-LC cannot be reliably mapped onto BoNT/C1-LC due to conformational and sequence differences. Nevertheless, the observation that the 250-loop of BoNT/C1-LC adopts a conformation similar to that observed in the substrate-bound BoNT/A-LC suggests that BoNT/C1-LC could potentially form β-exosite interactions with its substrates on the C-terminal side of the scissile bond.

On the N-terminal side of the scissile bond, the crystal structure of the BoNT/A-LC·SNAP-25 complex revealed a small loop (residues 183−190) that detaches from the surface of BoNT/A-LC (*14*). This loop may be able to accommodate the necessary "slack" for the cleavage bond register shift between BoNT/A and BoNT/C1 while maintaining the approximate position of the α-exosite. To test this hypothesis, we subjected this loop to insertions and deletions (Table 2). Upon insertion of up to three extra residues between Asp186

and Ser187 we observed largely unaltered cleavability and kinetic parameters for both BoNT/C1-LC and BoNT/A-LC. Likewise, deletion of Ser187, Ser187/Asn188, or Ser187-Lys189 did not affect SNAP-25 cleavability by BoNT/A-LC (Table 2). Interestingly, deletion of Ser187 significantly increased the cleavability of SNAP-25 by BoNT/C1-LC as indicated by a decrease in K_M and an increase in K_{cat} (Table 2). It is possible that the deletion of Ser187 brought the detached loop of SNAP-25 closer to the light chain and introduced extra interaction(s) in this region. For example, modeling showed that the deletion of Ser187 could bring Asn186 or Glu183 of SNAP-25 into favorable positions to interact with His25 of BoNT/C1-LC which might decrease the K_M value. Further deletions in this loop, up to three residues (Ser187-Lys189), consistently decreased the K_M values. We also observed a significantly increased K_{cat} value when Ser187 is deleted, which could probably be explained by the formation of a more efficient far-ranging substrate−enzyme interaction network involved in transition state stabilization, which is abated by further deletion (Table 2). Furthermore, mass spectrometry analyses showed that insertion or deletions in this region of SNAP-25 did not cause a shift of the scissile peptide bond (data not shown). Thus, there is no allosteric interaction via SNAP-25 between the exosites on both sides of this loop. Furthermore, the loop could provide the necessary slack to accommodate the register shift of the scissile bond for BoNT/A vs BoNT/C1 cleavage. Consistent with this notion, there is little effect upon insertion of up to three extra residues in this loop (Table 2). The divided roles for substrate discrimination among different exosites could provide some flexibility of the precise scissile bond position while ensuring high overall substrate specificity.

CONCLUSIONS

Understanding the mechanisms of substrate binding and cleavage by CNTs will provide important clues for vaccine and inhibitor development. On the other hand, modification of CNT-LC substrate specificities could produce novel clinical applications. With the crystal structure of BoNT/

C1-LC, all members of the family of CNT-LCs can now be compared in their apo form. All structures have a similar core structure with pronounced differences in surface exposed loops and key substrate interaction sites. We have identified a small putative S1′ pocket in BoNT/C1 that explains the strict dependence on an Ala residue at the P1′ site of its substrates. Although the α-exosite is largely conserved for the LCs of BoNT/A and BoNT/C1, the effects of substrate mutations that likely interact with this site are less pronounced for BoNT/C1 compared to BoNT/A. This less stringent requirement for the α-exosite interactions could be important for the dual substrate selectivity of BoNT/C1. There are other enzyme—substrate binding-sites: a substrate segment upstream of the α-exosite (*11*) and the scissile bond proximal exosites such as the β-exosite and the S1′ pocket. The S1′ pocket likely plays a key role in determining the correct register for the scissile bond. Our experiments also indicate a possible role of the protruding unstructured loop of SNAP-25 that was observed in the BoNT/A·SNAP-25 complex in accommodating the register shift between BoNT/A and BoNT/C1 LCs.

ACKNOWLEDGMENT

SUPPORTING INFORMATION AVAILABLE

The complete time course data showing hydrolysis of various SNAP-25 mutants by BoNT/C1-LC and BoNT/A-LC (supplementary Figure 1). This material is available free of charge via the Internet at http://pubs.acs.org.

REFERENCES

1. Burnett, J. C., Henchal, E. A., Schmaljohn, A. L., and Bavari, S. (2005) The evolving field of biodefence: therapeutic developments and diagnostics, *Nat. Rev. Drug Discovery 4*, 281−297.
2. Gill, D. M. (1982) Bacterial toxins: a table of lethal amounts, *Microbiol. Rev. 46*, 86−94.
3. Paddle, B. M. (2003) Therapy and prophylaxis of inhaled biological toxins, *J. Appl. Toxicol. 23*, 139−170.
4. Wein, L. M., and Liu, Y. (2005) Analyzing a bioterror attack on the food supply: the case of botulinum toxin in milk, *Proc. Natl. Acad. Sci. U.S.A. 102*, 9984−9989.
5. Jankovic, J. (2004) Botulinum toxin in clinical practice, *J. Neurol. Neurosurg. Psychiatry 75*, 951−957.
6. Turton, K., Chaddock, J. A., and Acharya, K. R. (2002) Botulinum and tetanus neurotoxins: structure, function and therapeutic utility, *Trends Biochem. Sci. 27*, 552−558.
7. Blasi, J., Chapman, E. R., Yamasaki, S., Binz, T., Niemann, H., and Jahn, R. (1993) Botulinum neurotoxin C1 blocks neurotransmitter release by means of cleaving HPC-1/syntaxin, *EMBO J. 12*, 4821−4828.
8. Schiavo, G., Shone, C. C., Bennett, M. K., Scheller, R. H., and Montecucco, C. (1995) Botulinum neurotoxin type C cleaves a single Lys-Ala bond within the carboxyl-terminal region of syntaxins, *J. Biol. Chem. 270*, 10566−10570.
9. Foran, P., Lawrence, G. W., Shone, C. C., Foster, K. A., and Dolly, J. O. (1996) Botulinum neurotoxin C1 cleaves both syntaxin and SNAP-25 in intact and permeabilized chromaffin cells: correlation with its blockade of catecholamine release, *Biochemistry 35*, 2630−2636.
10. Williamson, L. C., Halpern, J. L., Montecucco, C., Brown, J. E., and Neale, E. A. (1996) Clostridial neurotoxins and substrate proteolysis in intact neurons: botulinum neurotoxin C acts on synaptosomal-associated protein of 25 kDa, *J. Biol. Chem. 271*, 7694−7699.
11. Vaidyanathan, V. V., Yoshino, K., Jahnz, M., Dorries, C., Bade, S., Nauenburg, S., Niemann, H., and Binz, T. (1999) Proteolysis of SNAP-25 isoforms by botulinum neurotoxin types A, C, and E: domains and amino acid residues controlling the formation of enzyme-substrate complexes and cleavage, *J. Neurochem. 72*, 327−337.
12. Aktories, K., and Barth, H. (2004) The actin-ADP-ribosylating Clostridium botulinum C2 toxin, *Anaerobe 10*, 101−105.
13. Rossetto, O., Schiavo, G., Montecucco, C., Poulain, B., Deloye, F., Lozzi, L., and Shone, C. C. (1994) SNARE motif and neurotoxins, *Nature 372*, 415−416.
14. Breidenbach, M. A., and Brunger, A. T. (2004) Substrate recognition strategy for botulinum neurotoxin serotype A, *Nature 432*, 925−929.
15. Brunger, A. T. (2005) Structure and function of SNARE and SNARE-interacting proteins, *Q. Rev. Biophys. 38*, 1−47.
16. Eleopra, R., Tugnoli, V., Rossetto, O., Montecucco, C., and De, Grandis, D. (1997) Botulinum neurotoxin serotype C: a novel effective botulinum toxin therapy in human, *Neurosci. Lett. 224*, 91−94.
17. Eleopra, R., Tugnoli, V., Quatrale, R., Rossetto, O., and Montecucco, C. (2004) Different types of botulinum toxin in humans, *Mov. Disord. 19* (Suppl. 8), S53−S59.
18. Eleopra, R., Tugnoli, V., Quatrale, R., Rossetto, O., Montecucco, C., and Dressler, D. (2006) Clinical use of non-A botulinum toxins: botulinum toxin type C and botulinum toxin type F, *Neurotox. Res. 9*, 127−131.
19. Foran, P. G., Mohammed, N., Lisk, G. O., Nagwaney, S., Lawrence, G. W., Johnson, E., Smith, L., Aoki, K. R., and Dolly, J. O. (2003) Evaluation of the therapeutic usefulness of botulinum neurotoxin B, C1, E, and F compared with the long lasting type A. Basis for distinct durations of inhibition of exocytosis in central neurons, *J. Biol. Chem. 278*, 1363−1371.
20. Otwinowski, Z., and Minor, W. (1997) Processing of X-ray Diffraction Data Collected in Oscillation Mode, *Methods Enzymol. 276*, 307−326.
21. McCoy, A. J., Grosse-Kunstleve, R. W., Storoni, L. C., and Read, R. J. (2005) Likelihood-enhanced fast translation functions, *Acta Crystallogr., Sect. D: Biol. Crystallogr. 61*, 458−464.
22. Arndt, J. W., Chai, Q., Christian, T., and Stevens, R. C. (2006) Structure of botulinum neurotoxin type D light chain at 1.65 A resolution: repercussions for VAMP-2 substrate specificity, *Biochemistry 45*, 3255−3262.
23. Emsley, P., and Cowtan, K. (2004) Coot: model-building tools for molecular graphics, *Acta Crystallogr., Sect. D: Biol. Crystallogr. 60*, 2126−2132.
24. Brunger, A. T., Adams, P. D., Clore, G. M., DeLano, W. L., Gros, P., Grosse-Kunstleve, R. W., Jiang, J. S., Kuszewski, J., Nilges, M., Pannu, N. S., Read, R. J., Rice, L. M., Simonson, T., and Warren, G. L. (1998) Crystallography & NMR system: A new software suite for macromolecular structure determination, *Acta Crystallogr., Sect. D: Biol. Crystallogr. 54*, 905−921.
25. Brunger, A. T. (1992) Free R value: a novel statistical quantity for assessing the accuracy of crystal structures, *Nature 355*, 472−475.
26. Kleywegt, G. J. (1999) Experimental assessment of differences between related protein crystal structures, *Acta Crystallogr., Sect. D: Biol. Crystallogr. 55*, 1878−1884.
27. Krissinel, E., and Henrick, K. (2004) Secondary-structure matching (SSM), a new tool for fast protein structure alignment in three dimensions, *Acta Crystallogr., Sect. D: Biol. Crystallogr. 60*, 2256−2268.
28. Fenn, T. D., Ringe, D., and Petsko, G. A. (2003) POVScript+: a program for model and data visualization using persistence of vision ray-tracing, *J. Appl. Crystallogr. 36*, 944−947.
29. Holm, L., and Sander, C. (1993) Protein structure comparison by alignment of distance matrices, *J. Mol. Biol. 233*, 123−138.
30. Fu, Z., Chen, S., Baldwin, M. R., Boldt, G. E., Crawford, A., Janda, K. D., Barbieri, J. T., and Kim, J. J. (2006) Light chain of

botulinum neurotoxin serotype A: structural resolution of a catalytic intermediate, *Biochemistry 45*, 8903−8911.

31. Silvaggi, N. R., Boldt, G. E., Hixon, M. S., Kennedy, J. P., Tzipori, S., Janda, K. D., and Allen, K. N. (2007) Structures of Clostridium botulinum Neurotoxin Serotype A Light Chain Complexed with Small-Molecule Inhibitors Highlight Active-Site Flexibility, *Chem. Biol. 14*, 533−542.

32. Holden, H. M., Tronrud, D. E., Monzingo, A. F., Weaver, L. H., and Matthews, B. W. (1987) Slow- and fast-binding inhibitors of thermolysin display different modes of binding: crystallographic analysis of extended phosphonamidate transition-state analogues, *Biochemistry 26*, 8542−8553.

33. Agarwal, R., Binz, T., and Swaminathan, S. (2005) Structural analysis of botulinum neurotoxin serotype F light chain: implications on substrate binding and inhibitor design, *Biochemistry 44*, 11758−11765.

34. Arndt, J. W., Yu, W., Bi, F., and Stevens, R. C. (2005) Crystal structure of botulinum neurotoxin type G light chain: serotype divergence in substrate recognition, *Biochemistry 44*, 9574−9580.

35. Chen, S., and Barbieri, J. T. (2006) Unique substrate recognition by botulinum neurotoxins serotypes A and E, *J. Biol. Chem. 281*, 10906−10911.

36. Lacy, D. B., Tepp, W., Cohen, A. C., DasGupta, B. R., and Stevens, R. C. (1998) Crystal structure of botulinum neurotoxin type A and implications for toxicity, *Nat. Struct. Biol. 5*, 898−902.

37. Segelke, B., Knapp, M., Kadkhodayan, S., Balhorn, R., and Rupp, B. (2004) Crystal structure of Clostridium botulinum neurotoxin protease in a product-bound state: Evidence for noncanonical zinc protease activity, *Proc. Natl. Acad. Sci. U.S.A. 101*, 6888−6893.

38. Swaminathan, S., and Eswaramoorthy, S. (2000) Structural analysis of the catalytic and binding sites of Clostridium botulinum neurotoxin B, *Nat. Struct. Biol. 7*, 693−699.

39. Agarwal, R., Eswaramoorthy, S., Kumaran, D., Binz, T., and Swaminathan, S. (2004) Structural analysis of botulinum neurotoxin type E catalytic domain and its mutant Glu212→Gln reveals the pivotal role of the Glu212 carboxylate in the catalytic pathway, *Biochemistry 43*, 6637−6644.

40. Breidenbach, M. A., and Brunger, A. T. (2005) 2.3 A crystal structure of tetanus neurotoxin light chain, *Biochemistry 44*, 7450−7457.

41. Thompson, J. D., Higgins, D. G., and Gibson, T. J. (1994) CLUSTAL W: improving the sensitivity of progressive multiple sequence alignment through sequence weighting, position-specific gap penalties and weight matrix choice, *Nucleic Acids Res. 22*, 4673−4680.

42. Gouet, P., Courcelle, E., Stuart, D. I., and Metoz, F. (1999) ESPript: analysis of multiple sequence alignments in PostScript, *Bioinformatics 15*, 305−308.